Materials Science & Engineering C 108 (2020) 110405

Contents lists available at ScienceDirect

Materials Science & Engineering C

journal homepage: www.elsevier.com/locate/msec

Antifungal activity and biocompatibility of α-$AgVO_3$ microcrystals: A promising material against oral *Candida* disease

Bruna Natália Alves da Silva Pimentel[a,*], Camila Cristina de Foggi[a], Paula Aboud Barbugli[a], Regiane Cristina de Oliveira[b], Erica Dorigatti de Avila[a], Elson Longo[b], Carlos Eduardo Vergani[a]

[a] São Paulo State University (UNESP), School of Dentistry, Araraquara, Rua Humaita, 1680, 14801-903 Araraquara, SP, Brazil
[b] CDMF-UFSCar - Universidade Federal de São Carlos, Washington Luis km 235, P.O. Box 676, 13565-905 São Carlos, SP, Brazil

ARTICLE INFO

Keywords:
Candida albicans
Antifungal agents
Biocompatibility
Keratinocytes

ABSTRACT

The number of studies on microcrystals containing silver has increased in recent decades. Among the silver-containing microcrystals, α-$AgVO_3$ has gained prominence owing to its polymorphism that allows it to exert interesting antimicrobial activity against pathogenic microorganisms. The aim of this study was to evaluate the antifungal activity and cytotoxicity of three different α-$AgVO_3$ microcrystals when in solution. α-$AgVO_3$ microcrystals were synthesized using the co-precipitation method at three different temperatures (10 °C, 20 °C, and 30 °C), and then characterized by X-ray diffraction and scanning electron microscopy. The antifungal activity of α-$AgVO_3$ microcrystals against *Candida albicans* was determined by estimating the minimum inhibitory concentration (MIC) and minimum fungicidal concentration (MFC). Fluorescence images were obtained to confirm antifungal concentrations. To assess the biocompatibility of microcrystals applied at MIC and MFC on keratinocytes cells (NOK-si), an Alamar Blue assay, scanning electron microscopy, and a DNA gel integrity test were carried out. The quantitative and qualitative results showed that, regardless of the co-precipitation method used to synthetize α-$AgVO_3$ microcrystals, *C. albicans* growth was visibly inhibited at 3.9 μg/mL (MIC) and completely inhibited at 15.62 μg/mL (MFC). The cytotoxic and genotoxic outcomes revealed that the MIC and MFC concentrations did not affect NOK-si cell morphology, proliferation, or DNA integrity. The search for new antimicrobial materials has been the focus of the research community recently because of increases in microbial resistance. The findings reported herein demonstrate a novel antifungal and non-cytotoxic material that could be used in biomedical and dental applications.

1. Introduction

Infections caused by opportunistic fungi have emerged as a major cause of morbidity and mortality and remain a major public health challenge [1,2]. *Candida* species are commensal fungal that belong to the normal microbiota of the oral cavity, gastrointestinal tract, and vagina [2–6]. *Candida* spp. are responsible for over 90% of invasive fungal infections and *C. albicans* is present in approximately 40% of infections in the bloodstream [1,7]. When associated with local and/or systemic conditions, such as xerostomia, the use of dental prostheses, poor hygiene, chronic diseases, prolonged antibiotic therapy, or immunosuppression [5], *C. albicans* becomes virulent and can cause recurrent infections in the oral mucosa [5,8]. Further, *C. albicans* is responsible for generalized infections with high mortality rates [2,8,9].

Routine antifungal therapy includes local and/or systemic administration of drugs such as azoles, polyenes, and echinocandins, which have been associated with good clinical success [10]. However, the indiscriminate use of drugs has increased microbiology resistance, and thus, promoted increased failure of antifungal treatment. Collateral effects have also been documented as a result of prolonged use of these drugs, leading to liver and kidney damage [10]. Furthermore, the similarity between fungi and eukaryotic host cells restricts the panel of possible targets [11]. Thus, new therapies to inactivate pathogens have been widely researched during the last decade in order to minimize the development of resistance and the collateral effects of systemic toxicity [11–18].

Studies investigating novel strategies to prevent early infection and improve cell response (i.e. wound healing, angiogenesis) have shown instigating results [19–21]. In a recent report, Li et al. [19] developed an elastomeric material reinforced with inorganic nanowire of copper

* Corresponding author at: Department of Dental Materials and Prosthodontics, São Paulo State University (UNESP), School of Dentistry, Araraquara, Oral Rehabilitation Program, Rua Humaitá, 1680, Araraquara, São Paulo 14801-903, Brazil.
E-mail addresses: bruna.pimentel@yahoo.com.br (B.N.A.d.S. Pimentel), carlos.vergani@unesp.br (C.E. Vergani).

https://doi.org/10.1016/j.msec.2019.110405
Received 21 March 2019; Received in revised form 4 July 2019; Accepted 6 November 2019
Available online 07 November 2019
0928-4931/

sulfate disclosing antibacterial properties while still exhibiting good biocompatibility. In others notable findings, Zhou et al. [20] and Wang et al. [21] described two different hydrogels to address both challenges, limit microbial adhesion and stimulate target cell response to accelerate wound healing in vivo. The authors observed that the materials demonstrated antimicrobial activity against *Staphylococcus aureus* and *Escherichia coli* and were succeeded in improving angiogenesis in sick sites. A clear future direction for the new materials development is the capacity of effectively promoting interactions with host tissue cells while inhibiting microbial infection.

Silver has been widely studied for its antimicrobial properties [22]. However, growing concerns over the biosafety of silver concentration has limited the implementation of this metal in biomedical applications. Depending on the concentration, silver can induce an increased generation of reactive oxygen species (ROS), which consequently damages mammalian cell DNA. In addition, silver can be absorbed through cell membranes and accumulate in organs, such as liver, kidney, lung, brain, and skin [22]. To reduce the amount of silver used, researchers have combined silver with different metal oxides. Among a variety of compounds, silver vanadate ($AgVO_3$) has gained prominence because it contains less silver than other silver-containing compounds [16–18], which may increase its biocompatibility, making this a promising compound for use as a coating for the surfaces of biomedical devices and dental materials.

Silver vanadate ($AgVO_3$) is the most common form of the solid-state silver vanadate oxides [23] and can be found in three different forms: alpha (α), beta (β) and gamma (γ) [24]. Beta silver vanadate (β-$AgVO_3$) is a stable phase with a monoclinic space group [23] and is reported in the literature as a material with promising antibacterial activity against particular strains of Gram-positive and Gram-negative bacteria in solution [25]. When incorporated into the acrylic resin, this microcrystal reduces, significantly, the number of viable microorganisms of *C. albicans*, *Streptococcus mutans*, *Staphylococcus aureus* and *Pseudomonas aeruginosa* [26–28]. The alpha silver vanadate (α-$AgVO_3$) is a metastable phase, formed below the melting point instantaneously when the compound is slowly cooled and rapidly frozen [24]. Thus, polymorphism is prevalent in $AgVO_3$ which can result in different properties for each compound. Up to date, little is known about α-$AgVO_3$ antimicrobial properties and microbiological studies with this microcrystal are still scarce. Thus, the aim of this study was to evaluate the antifungal activity of alpha silver vanadate (α-$AgVO_3$) microcrystals against *C. albicans* and the effect of their suitable concentration on mammalian cells.

2. Material and methods

2.1. Synthesis and characterization of α-$AgVO_3$ microcrystals

The microcrystals were synthesized and characterized according to Oliveira et al. [29]. Briefly, 1 mmol of NH_4VO_3 and 1 mmol of $AgNO_3$ were separately diluted in 35 mL of water, under agitation, at a specific temperature (10 °C, 20 °C, or 30 °C). The solutions were mixed, and the microcrystals formed quickly. The microcrystals were washed with distilled water and dried in an oven (60 °C for 12 h). The α-$AgVO_3$ morphologies were investigated with a field emission scanning electron microscopy (FE-SEM) Supra 35-VP (Carl Zeiss, Oberkochen, Germany) operated in 15 KV. The microcrystals powders were characterized by X-ray diffraction using a Rigaku-DMax/2500PC (Rigaku, Tokyo, Japan) with Cu Kα radiation (λ = 1.5406 Å) in the 2θ range from 10° to 80° with a scanning rate of 0.02°/min.

2.2. Candida albicans culture and growth conditions

A standard strain of *C. albicans* (American Type Culture Collection – ATCC 90028) was used in this study. A loopful of a stock culture was streaked into a sabouraud dextrose agar (SDA, Himedia, Mumbai, India) plate and incubated under aerobic conditions at 37 °C. After 48 h, five colonies from the fresh grown culture were added to 10 mL of yeast nitrogen base (YNB, Himedia, Mumbai, India) and the pre-inoculum was maintained at 37 °C. Then, 500 μL of overnight culture were transferred to 9.5 mL of fresh YNB medium and the culture samples were incubated at 37 °C for 9 h. After incubation, the culture was harvested, washed once with sterile phosphate-buffered saline (PBS; pH 7.0) at 250*g* for 5 min, and resuspended in YNB medium. The optical density was adjusted to 0.55 at 540 nm, a value corresponding to the cell concentration of 1×10^6 CFU/mL in the log phase.

2.2.1. Antifungal activity of α-$AgVO_3$ microcrystals

To evaluate the antifungal activity, the minimum inhibitory concentration (MIC) and the minimum fungicidal concentration (MFC) against planktonic cells were determined using a broth microdilution method as described by the Clinical and Laboratory Standards Institute (CLSI), document M27-A3 [30]. MIC and MFC were determined by incubating of *C. albicans* at 1×10^3 CFU/mL directly into a 96-well polystyrene plate containing 100 μL of diluted microcrystals solution (serial dilution from 1000 to 0.97 μg/mL) for 24 h at 37 °C. To determine the MFC values, aliquots of 10-fold dilution (10^{-1} to 10^{-4}) of each well containing *C. albicans* and microcrystals at different concentrations were inoculated on SDA plates (10 μL), in duplicate, and incubated for 24 h at 37 °C. The results obtained as colony-forming units per milliliter (CFU/mL) were converted to Log value. *C. albicans* culture inoculated onto the plate served as the negative control. The experiments were performed in triplicate and in three independent occasions.

2.2.2. Fluorescence microscopy

MIC and MFC concentrations obtained against *C. albicans* were labeled with LIVE/DEAD BacLight™ Bacterial Viability Staining Kit (Invitrogen, Carlsbad, CA, USA), according to manufacturer's instructions. After 24 h of incubation of the microorganism with α-$AgVO_3$ microcrystals, the content of the wells was homogenized and 100 μL was transferred to a microtube. Then, 100 μL of LIVE/DEAD prepared reagent was inoculated into each microtube, homogenized, and maintained in a dark environment for at least 15 min. Finally, 10 μL of samples was pipetted onto a glass cover slip and visualized using a fluorescence microscopy LEICA DMI3000B (Leica, Wetzlar, Germany). *C. albicans* culture inoculated on the plate served as the negative control. This experiment was performed in duplicate in two independent occasions.

2.3. Keratinocyte cell culture and growth conditions

Normal oral keratinocyte spontaneously immortalized - NOK-si (kindly provided by Professor Carlos Rossa Junior, PhD, Department of Periodontics, Faculty of Dentistry of Araraquara – UNESP) [31] was used in this study. Cells were cultivated in Dulbecco's Modified Eagle's Medium (DMEM, GIBCO, Grand Island, NY, USA) with 2.0 mmol/L^{-1} glutamine supplemented with 10% of fetal bovine serum (FBS, GIBCO, Grand Island, NY, USA), penicillin G (10,000 μg.mL^{-1}), streptomycin (10,000 μg.mL^{-1}), and amphotericin (25 μg.mL^{-1}) (Sigma-Aldrich; St. Louis, MO, USA) in a humidified atmosphere of 5% CO_2 at 37 °C. Only the confluent NOK-si cells between the 3rd and 12th passage were harvested for further experiments.

2.3.1. Alamar Blue assay

The effect of the microcrystals on NOK-si cell proliferation was evaluated using an Alamar Blue assay. Cells were seeded onto 96-well polystyrene black plates (TPP® tissue culture plates, Trasadingen, Switzerland) at a concentration of 1×10^4 cells/well. The cells were incubated at 37 °C under 5% CO_2 conditions for 40 h. Subsequently, the medium was replaced with fresh medium containing microcrystals at MIC (C2) and MFC (C3) concentrations. Further concentrations were

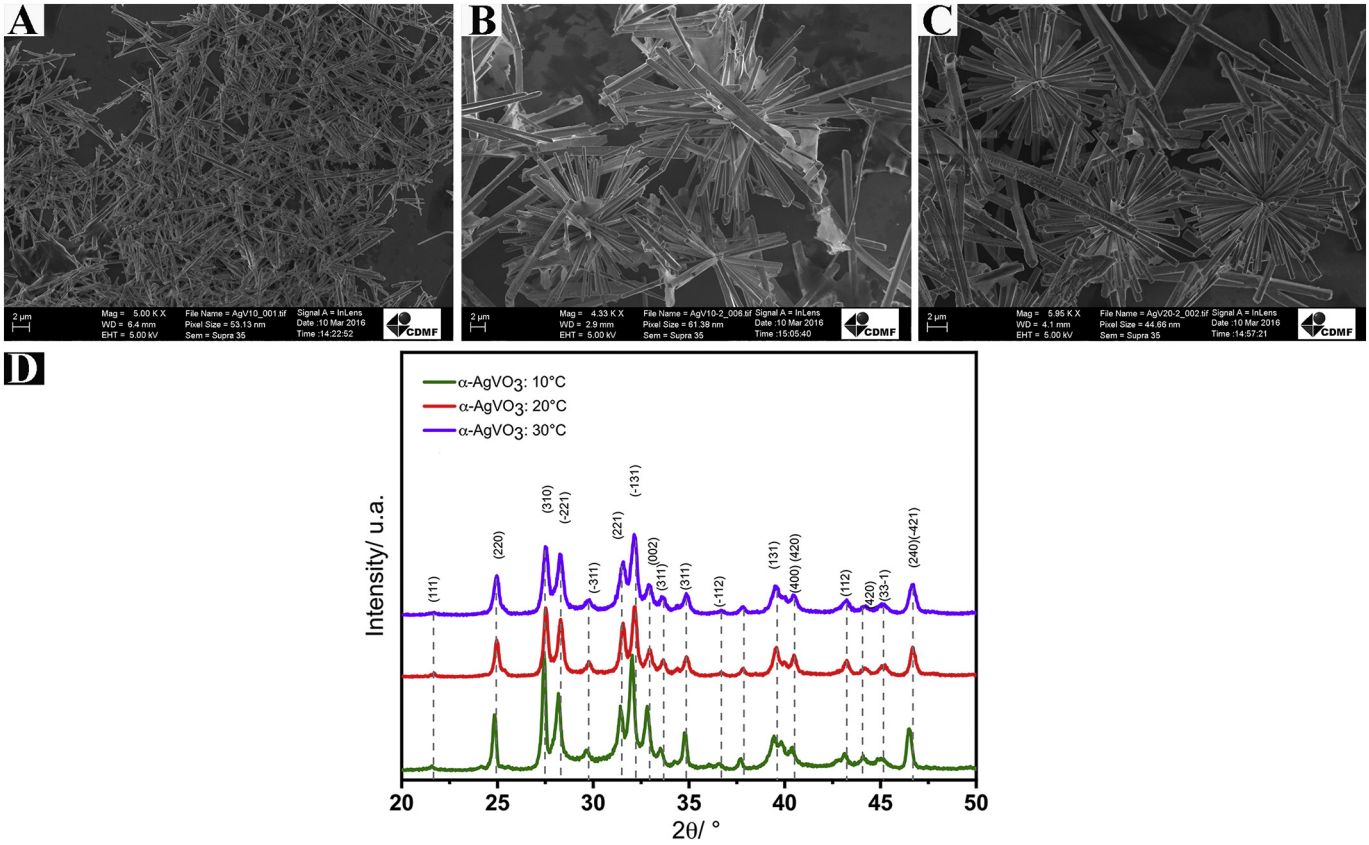

Fig. 1. Morphology of α-$AgVO_3$ microcrystals when synthesized at A) 10 °C revealed microrod structure; B) 20 °C and C) 30 °C revealed urchin-like morphologies; D) X-ray diffraction pattern for α-$AgVO_3$. The samples prepared at 10, 20, 30 °C showed similar peaks of the XRD patterns, which were readily indexed to a monoclinic phase α-$AgVO_3$, with space group C2/c (no. 15).

used as experimental references: MIC 10-fold diluted (C1) and MIC 10-fold concentrated (C4). Then, 10% Alamar Blue solution (Invitrogen, Carlsbad, CA, USA) was added to each well and the fluorescence (excitation 544 nm, emission 590 nm) was measured after 4 h, 6 h, 8 h, 12 h, and 24 h of incubation by fluorescence (Fluoroskan Ascent FL, ThermoScientific, Waltam, MA, USA). NOK-si cells under standard culture conditions without $AgVO_3$ microcrystals and cells incubated with 1% lysis solution (0.2% Triton x-100; Promega, Madison, WI, USA) were used as negative and positive controls, respectively. Wells in the same experimental conditions without cells were used as blank for all groups. This experiment was performed in sextuplicate and on three independent occasions.

2.3.2. SEM analysis

NOK-si cells were seeded onto a circular coverslip in a 24-well plate at a concentration of 6×10^4 cells/well. The plate was incubated at 37 °C for 48 h in order to establish a monolayer. Thereafter, the medium was replaced with fresh medium containing microcrystals at four different concentrations (C1 to C4) and maintained at 37 °C for 24 h. To determine the type of cell death based on cell morphology changes, cells were exposed to different cell death inducers and the morphology was compared to the negative control and experimental samples. Cells were incubated with camptotecin 20 mM (apoptosis inducer; Sigma-Aldrich, St. Louis, MO, USA) [32] for 4 h; hydrogen peroxide (H_2O_2) 6.45 M (necrosis inducer; Sigma-Aldrich, Duque de Caxias, RJ, Brazil) [33] for 20 min; and lysis solution (Triton x-100 0.2%; Promega, Madison, WI, USA) [34] for 5 min. After each incubation period, the medium was removed and the samples were prepared for SEM analysis. Briefly, samples were fixed with glutaraldehyde 2.5% for 60 min, followed by a progressive dehydration with alcohol (70%, 90%, and 100%). In sequence, samples were dried at room temperature, and stored in a vacuum desiccator for 5 to 7 days. Biological samples were coated with gold and SEM images were obtained at 200× magnification (JSM-6610LV, JEOL; Tokyo, Japan). Cells in standard culture conditions without α-$AgVO_3$ microcrystals were used as the negative control. This experiment was performed in duplicate and on two independent occasions.

2.3.3. DNA degradation test

Potential genotoxicity was confirmed by DNA integrity assessment after exposure of cells to different concentrations of microcrystals, as described previously by Haro-Chávez et al. [35]. Cells were cultured onto a 6-well plate at a concentration of 3.6×10^5 cells/well at 37 °C under 5% CO_2 conditions for 40 h. Subsequently, the medium was replaced with fresh medium containing microcrystals at four different concentrations (C1 to C4), and the plate was then maintained at 37 °C for 24 h. Thereafter, the cells were detached from the bottom of the plate and the washed-PBS pellet resuspended in 1.5 mL of PBS. To isolate the DNA, Master Pure DNA Purification kit (Epicenter, Madison, WI, USA) was used according to manufacturer's instructions. The DNA concentration obtained from each sample was quantified using a Nanodrop 2000 (ThermoScientific, Waltham, MA, USA), and the final amount of DNA normalized to 100 ng/μL. Then, 1% agarose gel stained with 3.2 μL of ethidium bromide (10 mg/mL) was prepared to load DNA samples. Nok-si cells under standard culture conditions without microcrystals were used as the negative control. This experiment was performed in duplicate and on two independent occasions.

2.4. Statistical analysis

In the present study, the concentration and morphology of microcrystals were considered to be a variation factor. After verifying the

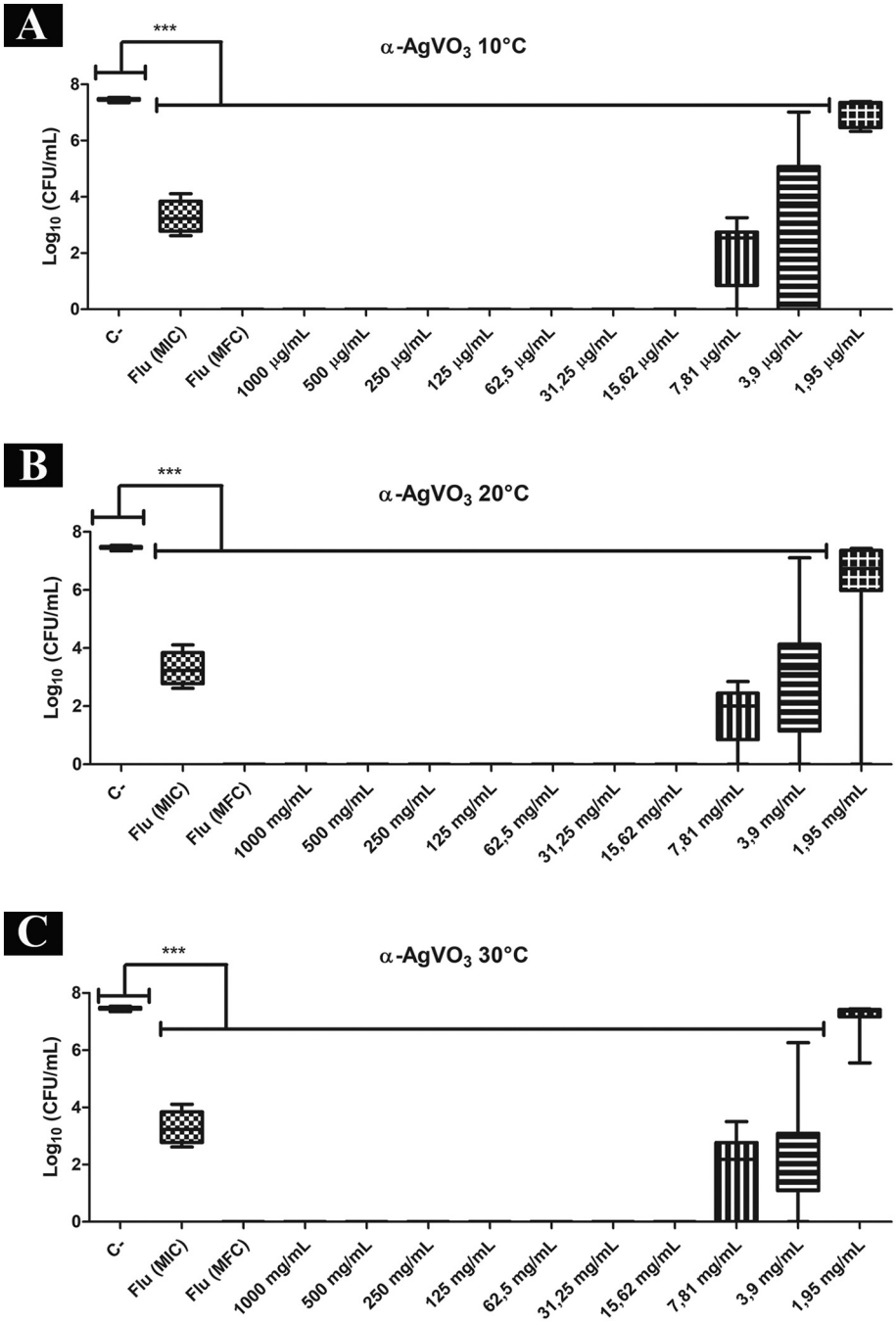

Fig. 2. Values of $\log_{10}$ (CFU/mL) of *C. albicans* suspensions treated with different concentrations of α-$AgVO_3$ obtained at 10 °C (A); 20 °C (B); 30 °C (C). Flu: Fluoconazole; Flu (MIC): 64 μg/mL; Flu (MFC): 256 μg/mL; Dot: median; Square upper limit: 3rd quartile; Square lower limit: 1st quartile; Bars: maximum and minimum values. (n = 9); ***$p < 0.0001$ was considered statistically significant when compared with the control (C-).

normal and homogeneous distributions of data, Kruskal-Wallis test, followed by Dunn's test (α = 0.05), was performed. Statistical analysis was carried out using GraphPad Prism 7 (La Jolla, CA, USA).

3. Results and Discussion

3.1. Structural and morphological characterization of α-$AgVO_3$ microcrystals

To determine how temperature affects the morphology, structure, composition, and physical properties of α-$AgVO_3$, microcrystals were synthetized at 10, 20 and 30 °C. Regardless of the temperature, overall α-$AgVO_3$ morphology revealed uniform size distribution of particles. Microcrystals synthetized at 10 °C showed microrod of α-$AgVO_3$ and well defined faces (Fig. 1A). With the temperature increase at 20 °C occurred a direct self-assembly of nanorods to form urchin-like microspheres (Fig. 1B). At 30 °C, α-$AgVO_3$ microcrystals disclosed predominantly urchin-like morphologies (Fig. 1C). The crystallinity of α-$AgVO_3$ powder synthetized at different temperatures was identified by XRD spectra (Fig. 1D). The samples prepared at 10, 20, 30 °C showed similar peaks of the XRD patterns, which were readily indexed to a monoclinic phase α-$AgVO_3$, with space group C2/c (no. 15). All the diffraction peaks are well accordant with Inorganic Crystal Structure Database (ICSD) pattern no. 50645 and indicate the high phase purity in the three samples.

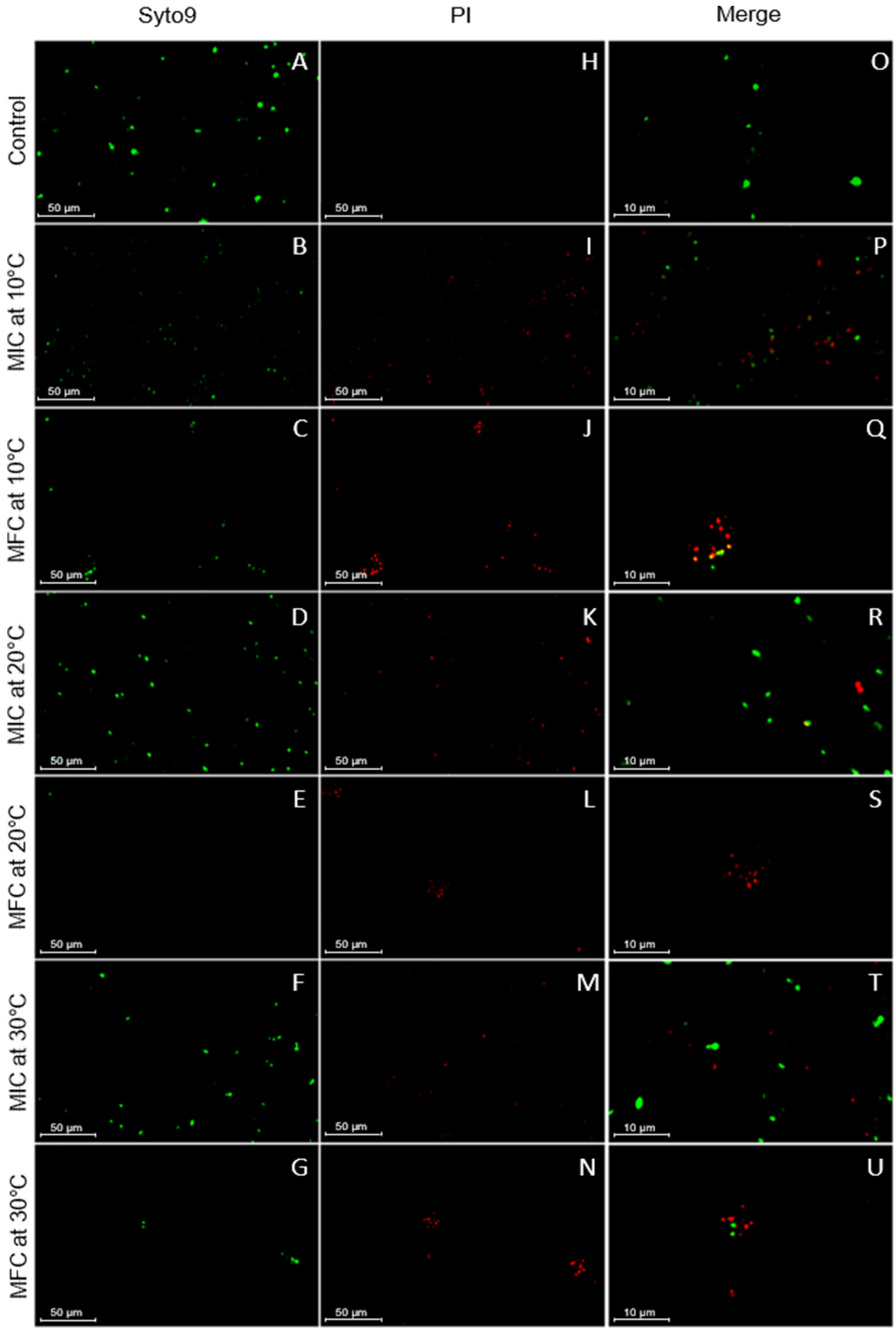

(caption on next page)

Fig. 3. Fluorescence microscopy. (A, B, C) Control (*C. albicans* in culture medium). (D, E, F) *C. albicans* in contact with α-$AgVO_3$, synthesized at 10 °C, at MIC. (G, H, I) *C. albicans* in contact with α-$AgVO_3$, synthesized at 10 °C, at MFC. (J, K, L) *C. albicans* in contact with α-$AgVO_3$, synthesized at 20 °C, at MIC.(M, N, O) *C. albicans* in contact with α-$AgVO_3$, synthesized at 20 °C, at MFC·(P, Q, R) *C. albicans* in contact with α-$AgVO_3$, synthesized at 30 °C, at MIC. (S, T, U) *C. albicans* in contact with α-$AgVO_3$, synthesized at 30 °C, at MFC. Merge images are in approximate view.

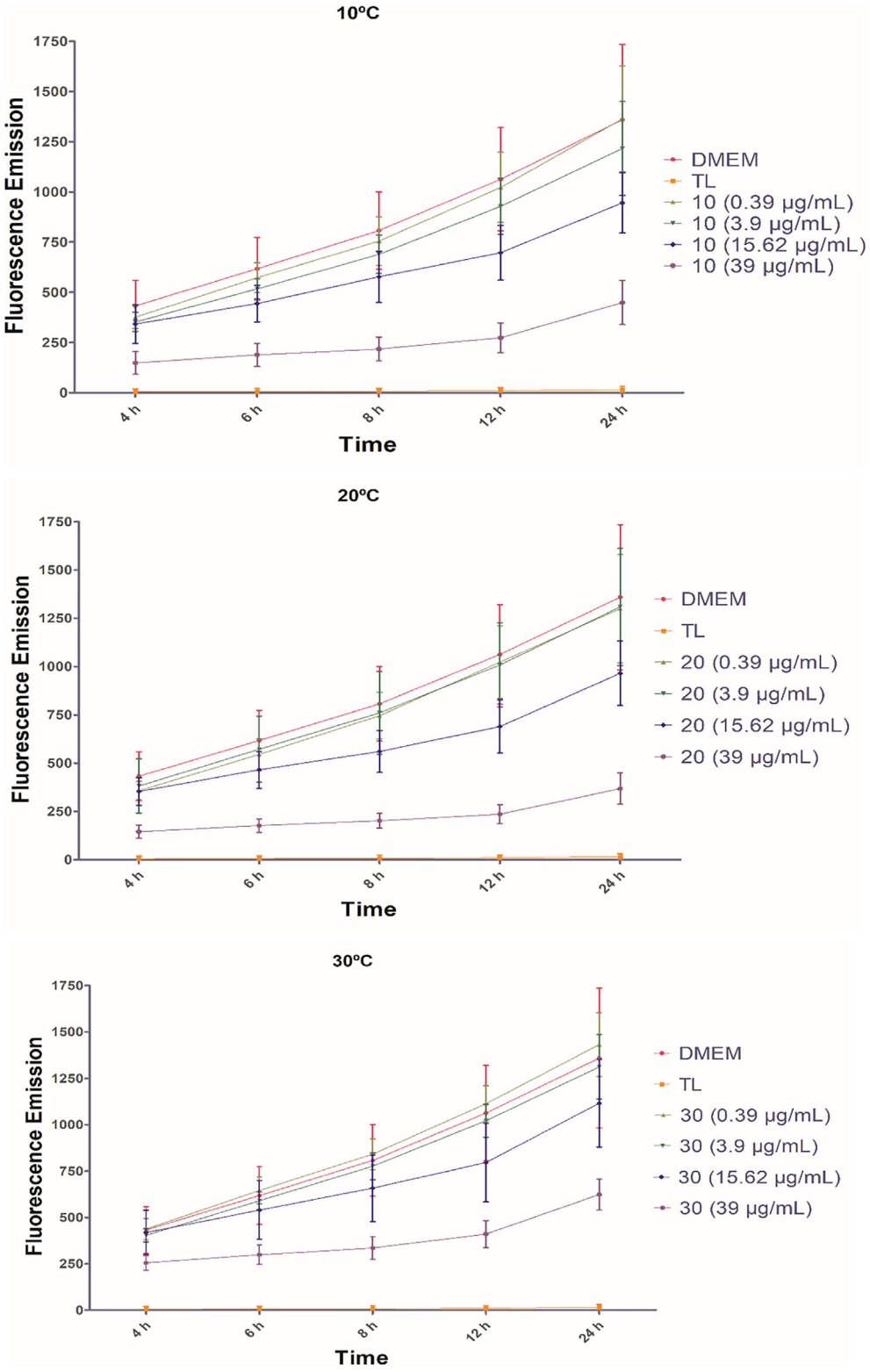

Fig. 4. Mean values of fluorescence emission (544 nm/590 nm) indicating cell proliferation in contact with different concentrations of α-$AgVO_3$ at 10 °C, 20 °C, and 30 °C, at different times (2 h, 4 h, 6 h, 8 h, 12 h and 24 h). DMEM is the negative control. TL (Lysis solution) is the positive control. Error bars represent the standard deviation.

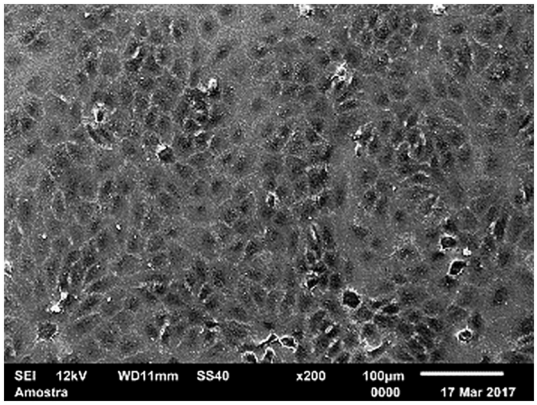

Fig. 5. SEM image of NOK-si cells cultivated in DMEM. Magnification 200×.

3.2. Antifungal activity

The results demonstrated that, regardless of the temperature used to synthetize α-$AgVO_3$, microcrystals presented fungistatic and fungicidal activity against *C. albicans*. Furthermore, although the microcrystals presented different morphologies, all exhibited the same values of MIC and MFC (3.9 µg/mL and 15.62 µg/mL, respectively). It is important to note that, even at sub-MIC concentrations, all three microcrystals were capable of reducing yeast growth (Fig. 2). When in standard culture conditions (negative control), *C. albicans* presented 7.46 $\log_{10}$ CFU/mL, whereas when incubated with half MFC concentration (7.81 µg/mL), there was an inhibition of approximately 1.97 $\log_{10}$ CFU/mL, 1.74 $\log_{10}$ CFU/mL, and 1.49 $\log_{10}$ CFU/mL for α-$AgVO_3$ obtained at 10 °C, 20 °C, and 30 °C, respectively. To confirm the results obtained using the CFU/mL method, fluorescence microscopy was performed by staining the microorganism after contact with microcrystals at MIC and MFC (Fig. 3). The first column of Fig. 3 shows microorganisms stained with syto9 (Fig. 3A–G) indicating the presence of fungal cells. The second column shows microorganisms stained with propidium iodide (Fig. 3H–N). It is possible to note that at MIC for all three microcrystals only some microorganism cells were stained with propidium iodide (Fig. 3I, K and M), indicating that the microbial cell wall was disrupted. However, Fig. 3(J, L and N) also shows that all microorganism cells were stained with propidium iodide. The third column shows an approximated view of merge images (Fig. 3O–U), where is possible to better view the difference between groups. These results suggest that α-$AgVO_3$ microcrystals had a great antifungal activity against *C. albicans*.

In a recent study [29], the microcrystals used in this study were tested against methicillin-resistant *Staphylococcus aureus* (MRSA). The MIC and minimum bactericidal concentration (MBC) values obtained for MRSA were higher than the values against *C. albicans* (62.5 µg/mL at 10 °C, 125 µg/mL at 20 °C and 30 °C). According to Oliveira et al. [29], α-$AgVO_3$ microcrystals act through the oxidative stress resulting from the production of reactive oxygen species (ROS), such as OH*, O_2', and O_2H*. The differences between the MIC and MFC/MBC values found for *C. albicans* and MRSA can be explained by the morphological and structural differences between these two microorganisms. In Gram-positive bacteria, such as MRSA, there is no outer membrane, the peptidoglycan cell wall is thick (20–50 nm), and the chains of teichoic acid cross the cell wall [36,37], whereas *C. albicans* consist of (1,3)-β-D-glucans linked to (1,6)-β-D glucans, chitin, and ergosterol [6]. This difference in the biochemical composition of the cell walls may have contributed to the differences in behavior between the two microorganisms, since lipids are oxidized faster than carbohydrates [38]. In addition, because the concentrations necessary to eliminate *C. albicans* are too small, the morphology of the microcrystals may not have been crucial for MIC and MFC.

Other studies on the antifungal activity of microcrystals containing

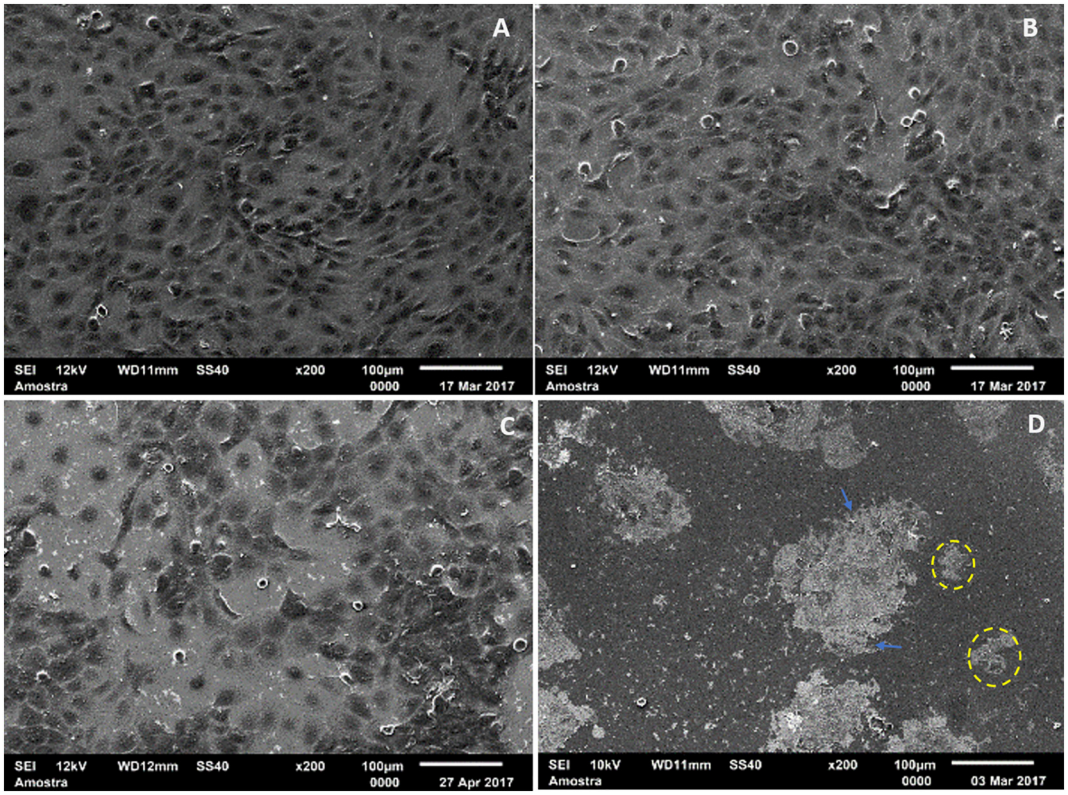

Fig. 6. SEM images of NOK-si cells after 24 h contact with different concentrations of α-$AgVO_3$ synthesized at 10 °C. Cells + microcrystals at (A) C1, (B) C2, (C) C3, and (D) C4. Blue arrows indicate membrane disruption; yellow dashes indicate increased cytoplasmic volume. Magnification 200×. (For interpretation of the references to colour in this figure legend, the reader is referred to the web version of this article.)

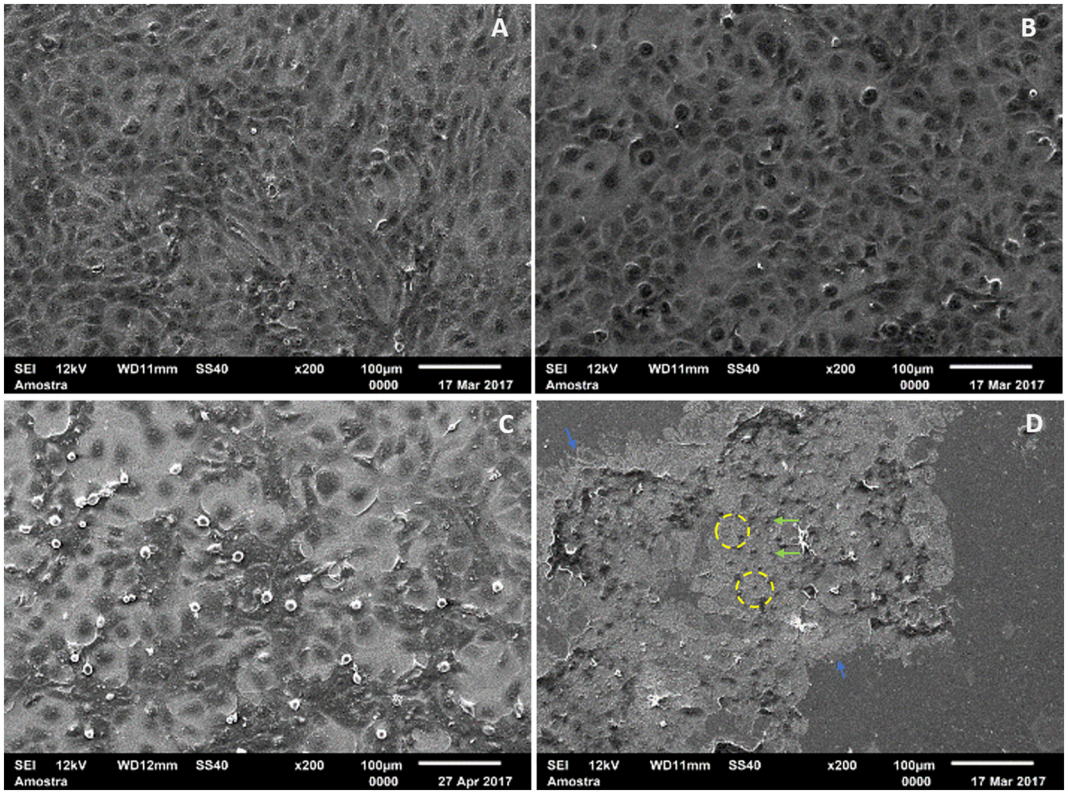

Fig. 7. SEM images of NOK-si cells after 24 h contact with different concentrations of α-$AgVO_3$ synthesized at 20 °C. Cells + microcrystals at (A) C1, (B) C2, (C) C3, and (D) C4. Blue arrows indicate membrane disruption; yellow dashes indicate increased cytoplasmic volume; green arrows indicate pyknotic cell nucleus. Magnification 200×. (For interpretation of the references to colour in this figure legend, the reader is referred to the web version of this article.)

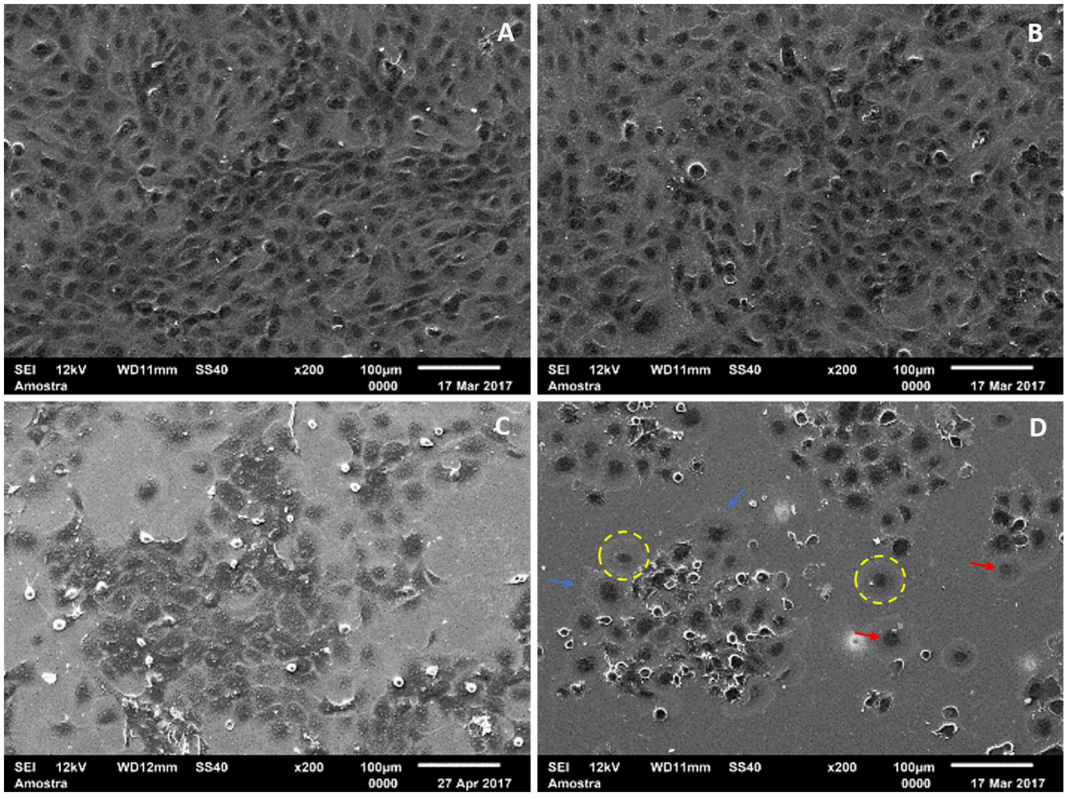

Fig. 8. SEM images of NOK-si cells after 24 h contact with different concentrations of α-$AgVO_3$ synthesized at 30 °C. Cells + microcrystals at (A) C1, (B) C2, (C) C3, (D) C4. Blue arrows indicate membrane disruption; yellow dashes indicate increased cytoplasmic volume; red arrows indicate nuclei in karyolysis. Magnification 200×. (For interpretation of the references to colour in this figure legend, the reader is referred to the web version of this article.)

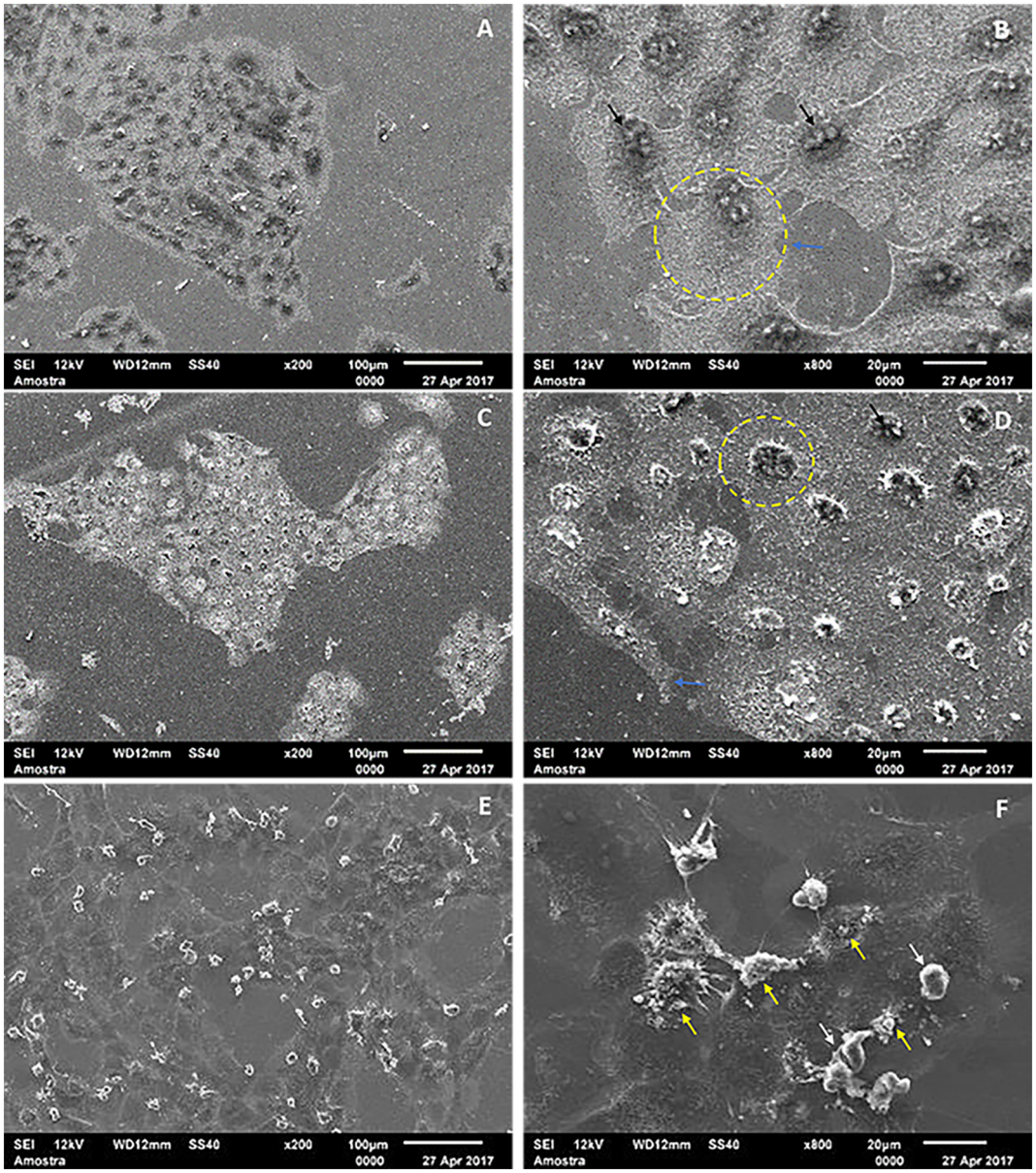

Fig. 9. SEM images of NOK-si cells after contact with H_2O_2 (A, B); Triton x-100 (C, D); and camptotecin (E, F). Yellow arrows indicate the apoptotic bodies; white arrows indicate the maintenance of the membrane integrity; blue arrows indicate membrane disruption; black arrows indicate nuclei in karyorrhexis; yellow dashes indicate increased cytoplasmic volume. Magnification 200× (left column); 800× (right column). (For interpretation of the references to colour in this figure legend, the reader is referred to the web version of this article.)

silver against *C. albicans* (ATCC 90028) have recently been published [16,18]. In their studies, Foggi et al. [18] and Fabbro et al. [16] obtained the same MIC value (3.9 µg/mL) as α-$AgVO_3$, and the amount of silver released by the three particles were very similar: 0.017 µmol/mL, 0.021 µmol/mL, and 0.019 µmol/mL, respectively.

The literature reports other studies where antimicrobial activity of several compounds (organic or inorganic) have been evaluated. Shakibaie et al. [39] evaluated the antifungal potential of selenium nanoparticles against *Candida albicans* and it was found a MIC of 70 µg/mL, which is almost 18-folds the MIC found in the present study. In addition, the authors did not evaluate the biocompatibility of these nanoparticles. In a literature review, Teodoro et al. [40], have compared different studies, which evaluated antifungal activity of phenolic acids derived from natural sources against *Candida* spp. The authors have observed that the MIC of phenolic acids is highly variable, ranging from 7.28 µg/mL to 12,500 µg/mL. It is important to highlight that these range of MIC values were obtained to different species and strains of *Candida*, which makes it difficult to compare data.

3.3. Biocompatibility

The effect of α-$AgVO_3$ microcrystals on NOK-si cells from 4 to 24 h was investigated using an Alamar Blue assay. At C1 and C2, there were no significant differences in cell viability when compared with the negative control (Nok-si with DMEM), regardless of the time point or the microcrystal synthesis method (Fig. 4). At C3, no differences with the negative control were observed for any of the three microcrystals at 4 and 24 h; for α-$AgVO_3$ synthesized at 20 °C and 30 °C, there was no difference at 6 h. At the other two time points (8 h and 12 h), a significant difference was noted (α-$AgVO_3$ synthesized at 10 °C: $p = 0.0421$ and $p = 0.0150$, respectively; α-$AgVO_3$ synthesized at 20 °C: $p = 0.0147$ and $p = 0.0133$, respectively) when C3 was compared against the negative control, except for α-$AgVO_3$ synthesized at 30 °C. A cytotoxic effect was observed when the cells were maintained

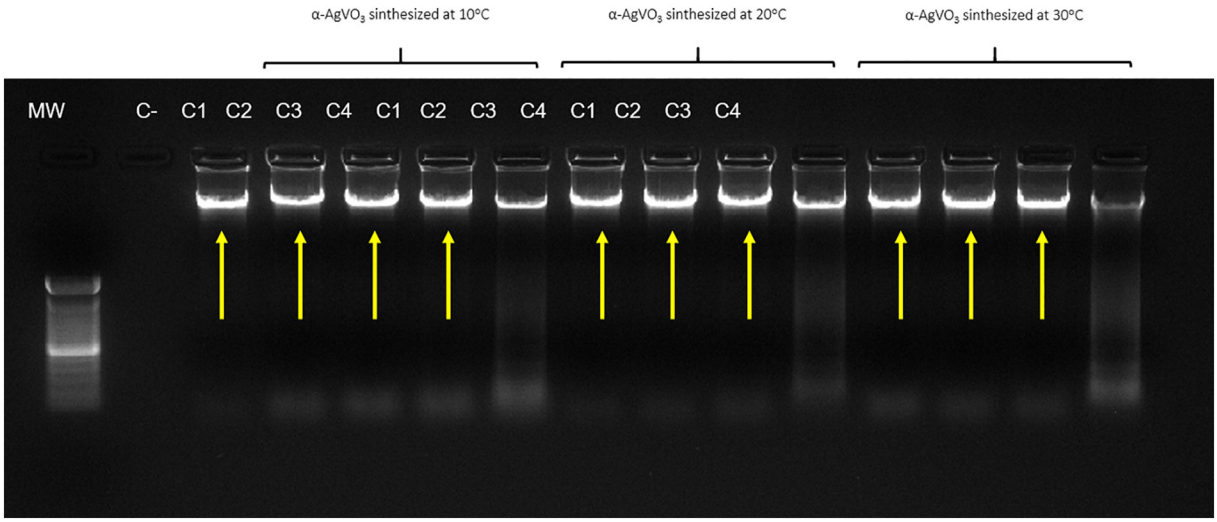

Fig. 10. Agarose gel electrophoresis for separation of DNA fragments. The negative control group (C^-) and the concentrations C1, C2, and C3 presented only one band (yellow arrows), confirming that α-$AgVO_3$ at those concentrations did not compromise DNA integrity. The positive control (C^+) group, which was the C4 concentration, demonstrates the presence of different bands, indicating the fragmentation of the molecule. The images are representative of experiments performed in duplicate and on two different occasions. MW: molecular weight. (For interpretation of the references to colour in this figure legend, the reader is referred to the web version of this article.)

in contact with the highest concentrations (C4).

From the SEM images, it was possible to note that cell morphology correlated well with the Alamar Blue findings. Cells exposed to C1, C2, and C3 concentrations showed morphology very similar to the cells of the negative control, indicating the biocompatibility of microcrystals even after 24 h of contact (Figs. 5, 6A–C, 7A–C, 8A–C). On the contrary, cells maintained in contact with C4 concentration showed a morphology very similar to cell death by necrosis (Figs. 6D, 7D, 8D), due to the great similarity to cell necrosis morphology induced by the controls Triton x-100 and H_2O_2 (Fig. 9A–D). In this case, it was possible to observe cell alterations typical of the necrotic process, such as increased cytoplasmic volume, pyknotic nucleus (in karyorrhexis or in karyolysis), damaged cell membrane, and cellular extravasation [41]. A control induced by camptotecin (apoptosis) showed apoptotic cell death characterized by membrane integrity, reduced cytoplasm, and the formation of apoptotic bodies [41] (Fig. 9E–F).

It is well known that ROS are extremely reactive and lead to DNA damage [42]. Thus, in attempt to confirm the non-cytotoxic properties of α-$AgVO_3$ on mammalian cells, we also investigated effect of different microcrystal morphologies on DNA integrity. The results revealed that after 24 h of contact, intact DNA bands were observed at the concentrations C1, C2, and C3, as well as in the negative control (Fig. 10). On the other hand, cells in contact with C4 concentration showed DNA drag. These results were consistent with our previous results where C4 concentration was found to induce toxicity in cells.

In recent years, silver-containing microcrystals have been widely studied because of their superior characteristics, especially with regards to biocompatibility relative to silver-containing nanoparticles [16,18,22,29,35,43]. Silver-containing metal particles of larger sizes were able to maintain the positive properties of the silver nanoparticles, as antimicrobial agents, but allowed for the improvement of the biocompatibility of the compounds. The toxic concentration of silver nanoparticles on eukaryotic cells in vitro has been reported to be around 10–100 mg/L after 24 h of contact [44]. Our results showed that the target concentrations of 3.9 μg/mL and 15.62 μg/mL, containing 0.019 μmol/mL and 0.076 μmol/mL, respectively, did not affect the cells proliferation and morphology, even after 24 h of contact.

4. Conclusion

α-$AgVO_3$ microcrystals showed antifungal activity, and their MIC and MFC values demonstrated that they are not cytotoxic against keratinocyte cells, regardless of morphological variations on the microcrystals. The results described here provide evidence of a novel and safe antimicrobial compound for use in biomedical and dental applications.

Acknowledgements

This work was supported by the São Paulo Research Foundation (FAPESP) [grant numbers 2015/25124-0; and CDMF: 2013/07296-2]. Bruna Natália Alves da Silva Pimentel was supported by FAPESP [grant number 2015/13834-2]. Camila Cristina de Foggi was supported by FAPESP [grant number 2015/03654-7]. Erica Dorigatti de Avila was supported by FAPESP [grant number 2015/03567-7].

References

[1] M. Masiá Canuto, F. Gutiérrez Rodero, Antifungal drug resistance to azoles and polyenes, Lancet Infect. Dis. 2 (2002) 550–563.
[2] J.C.O. Sardi, L. Scorzoni, T. Bernardi, A.M. Fusco-Almeida, M.J.S. Mendes-Giannini, *Candida* species: current epidemiology, pathogenicity, biofilm formation, natural antifungal products and new therapeutic options, J. Med. Microbiol. 62 (2013) 10–24.
[3] M. Avila, D.M. Ojcus, O. Yilmaz, The oral microbiota: living with a permanent guest, DNA Cell Biol. 28 (2009) 405–411.
[4] M.E. Shirtliff, B.M. Peters, M.A. Jabra-Rizk, Cross-kingdom interactions: *Candida albicans* and bacteria, FEMS Microbiol. Lett. 299 (2009) 1–8.
[5] C. Salerno, M. Pascale, M. Contaldo, V. Esposito, M. Busciolano, L. Milillo, et al., *Candida*-associated denture stomatitis, Med. Oral Patol. Oral Cir. Bucal. 16 (2011) 139–143.
[6] R.S. Shapiro, N. Robbins, L.E. Cowen, Regulatory circuitry governing development, drug resistance, and disease, Microbiol. Mol. Biol. Rev. 75 (2011) 213–267.
[7] M.A. Pfaller, D.J. Diekema, G.W. Procop, M.G. Rinaldi, Multicenter comparison of the VITEK 2 antifungal susceptibility test with the CLSI broth microdilution reference method for testing amphotericin B, Flucytosine, and voriconazole against *Candida* spp. J. Clin. Microbiol. 45 (2007) 3522–3528.
[8] P. Sudbery, N. Gow, J. Berman, The distinct morphogenic states of *Candida albicans*, Trends Microbiol. 12 (2004) 317–324.
[9] M. Gulati, C.J. Nobile, *Candida albicans* biofilms: development, regulation, and molecular mechanisms, Microbes Infect. 18 (2016) 310–321.
[10] V.T. Andriole, Current and future antifungal therapy: new targets for antifungal therapy, Int. J. Antimicrob. Agents 16 (2000) 317–321.
[11] K.J. Kim, W.S. Sung, B.K. Suh, S.K. Moon, J.S. Choi, J.G. Kim, et al., Antifungal activity and mode of action of silver nano-particles on *Candida albicans*, Biometals 22 (2009) 235–242.
[12] A. Panacek, M. Kolar, R. Vecerova, R. Prucek, J. Soukupová, V. Krystof, et al., Antifungal activity of silver nanoparticles against Candida spp. Biomaterials 30 (2009) 6333–6340.
[13] A. Lipovsky, Y. Nitzan, A. Gedanken, R. Lubart, Antifungal activity of ZnO

nanoparticles – the role of ROS mediated cell injury, Nanotechnology 22 (10) (2011) 105101.
[14] J.C. Junqueira, A.O.C. Jorge, J.O. Barbosa, R.D. Rossoni, S.F.G. Vilela, A.C.B.P. Costa, et al., Photodynamic inactivation of biofilms formed by *Candida* spp., *Trichosporon mucoides*, and *Kodamaea ohmeri* by cationic nanoemulsion of zinc 2,9,16,23-tetrakis (phenylthio)-29H, 31H-phthalocyanine (ZnPc), Lasers Med. Sci. 27 (2012) 1205–1212.
[15] L.N. Dovigo, J.C. Carmello, M.T. Carvalho, E.G. Mima, C.E. Vergani, V.S. Bagnato, et al., Photodynamic inactivation of clinical isolates of *Candida* using Photodithazine®, Biofouling 29 (2013) 1057–1067.
[16] M.T. Fabbro, C.C. Foggi, L.P.S. Santos, L. Gracia, A. Perrin, C. Perrin, et al., Synthesis, antifungal evaluation and optical properties of silver molybdate microcrystals in different solventes: a combined experimental and theoretical study, Dalton Trans. 45 (2016) 10736–10743.
[17] C.C. Foggi, M.T. Fabbro, L.P.S. Santos, Y.V.B. Santana, C.E. Vergani, A.L. Machado, et al., Synthesis and evaluation of α-Ag2WO4 as novel antifungal agent, Chem. Phys. Lett. 624 (2017) 125–129.
[18] C.C. De Foggi, R.C. De Oliveira, M.T. Fabbro, C.E. Vergani, J. Andrés, E. Longo, et al., Tuning the morphological, optical, and antimicrobial properties of α-Ag_2WO_4 microcrystals using different solvents, Cryst. Growth Des. 17 (2017) 6239–6246.
[19] Y. Li, N. Li, J. Ge, Y. Xue, W. Niu, M. Chen, et al., Biodegradable thermal imaging-tracked ultralong nanowire-reinforced conductive nanocomposites elastomers with intrinsical efficient antibacterial and anticancer activity for enhanced biomedical application potential, Biomaterials 201 (2019) 68–76.
[20] L. Zhou, Y. Xi, Y. Xue, M. Wang, Y. Liu, Y. Guo, et al., Injectable self-healing antibacterial bioactive polypeptide-based hybrid nanosystems for efficiently treating multidrug resistant infection, skin-tumor therapy, and enhancing wound healing, Adv. Funct. Mater. 29 (22) (2019) 1806883.
[21] C. Wang, M. Wang, T. Xu, X. Zhang, C. Lin, W. Gao, et al., Engineering bioactive self-healing antibacterial exosomes hydrogel for promoting chronic diabetic wound healing and complete skin regeneration, Theranostics 9 (1) (2019) 65–76.
[22] A.D. Politano, K.T. Campbell, L.H. Rosenberger, R.G. Sawyer, Use of silver in the prevention and treatment of infections: silver review, Surg. Infect. 14 (2013) 8–20.
[23] K.J. Takeuchi, A.C. Marschilok, S.M. Davis, E.S. Leising RA Takeuchi, Silver vanadium oxides and related battery applications, Coord. Chem. Rev. (2001) 283–310.
[24] K. Shigeharu, M. Kosaku, A. Haruo, Crystal structure of alpha-AgVO3 and phase relation of AgVO3, J. Solid State Chem. 142 (1999) 360–367.
[25] R.D. Holtz, B.A. Lima, A.G. Souza Filho, M. Brocchi, O.L. Alves, Nanostructured silver vanadate as a promising antibacterial additive to water-based paints, Nanomed. Nanotechnol. Biol. Med. (2012) 935–940.
[26] D.T. Castro, R.D. Holtz, O.L. Alves, E. Watanabe, M.L.C. Valente, C.H.L. Silva, et al., Development of a novel resin with antimicrobial properties for dental application, J. Appl. Oral Sci. 22 (5) (2014) 442–449.
[27] D.T. Castro, M.L.C. Valente, J.A.M. Agnelli, C.H.L. Silva, E. Watanabe, R.L. Siqueira, et al., In vitro study on the antibacterial properties and impact strength of dental acrylic resins modified with a nanomaterial, J. Prosthet. Dent. 115 (2016) 238–246.
[28] D.T. Castro, M.L.C. Valente, C.H.L. Silva, E. Watanabe, R.L. Siqueira, M.A. Schiavon, et al., Evaluation of antibiofilm and mechanical properties of new nanocomposites based on acrylic resins and silver vanadate nanoparticles, Arch. Oral Biol. (2016) 46–53.
[29] R.C. Oliveira, C.C. Foggi, M.M. Teixeira, M.D.P. Silva, M. Assis, E.M. Francisco, et al., Mechanism of antibacterial activity via morphology change of α-$AgVO_3$: theoretical and experimental insights, ACS Appl. Mater. Interfaces 9 (2017) 11472–11481.
[30] CLSI, Reference Method for Broth Dilution Antifungal Susceptibility Testing of Yeasts; Approved Standard, 3rd ed., Clinical and Laboratory Standards Institute, Wayne, PA, 2008http://www.anvisa.gov.br/servicosaude/manuais/clsi/clsi_OPAS1M27-A2.pdf , Accessed date: 1 April 2016(CLSI Document M27-A2).
[31] R.M. Castilho, C.H. Squarize, K. Leelahavanichkul, Y. Zheng, T. Bugge, J.S. Gutkind, Rac1 is required for epithelial stem cell function during dermal and oral mucosal wound healing but not for tissue homeostasis in mice, PLoS One 5 (2010) e10503.
[32] BDBioscience – support protocol BD, http://www.bdbiosciences.com/in/resources/protocols/cell_death.jsp , Accessed date: 1 April 2017.
[33] A.M.A. Mohammad, D.K. Arulmozhi, F. Xiaohu, R. Schultz, Hydrogen peroxide-induced necrotic cell death in cardiomyocytes is independent of matrix metalloproteinase-2, Toxicol. in Vitro 27 (2013) 1686–1692.
[34] R. Hoffman, In vitro toxicology and cellular fate determination using promega's cell-based assays, Cell Notes Issue (2002), https://www.promega.com.br/resources/pubhub/cellnotes/in-vitro-toxicology-and-cellular-fate-determination-using-promega-cell-based-assays/ , Accessed date: 1 April 2017.
[35] N.L. Haro Chávez, E.D. de Avila, P.A. Barbugli, R.C. de Oliveira, C.C. de Foggi, E. Longo, et al., Promising effects of silver tungstate microcrystals on fibroblast human cells and three dimensional collagen matrix models: a novel non-cytotoxic material to fight oral disease, Colloids Surf. B: Biointerfaces 170 (2018) 505–513.
[36] S. Brown, J.P. Santa Maria Jr., S. Walker, Wall teichoic acids of gram-positive bacteria, Annu. Rev. Microbiol. 67 (2013) 313–336.
[37] M.G. Percy, A. Gründling, Lipoteichoic acid synthesis and function in gram-positive bacteria, Annu. Rev. Microbiol. 68 (2014) 81–100.
[38] D.L. Nelson, M.M. Cox, Catabolism of fatty acids, in: D.L. Nelson, M.M. Cox (Eds.), Lehninger Principles of Biochemistry, 6th edition, vol. 17, Artmed, Porto Alegre, 2014, pp. 667–694.
[39] M. Shakibaie, N.S. Mohazab, S.A.A. Mousavi, Antifungal activity of selenium nanoparticles synthesized by *Bacillus species* Msh-1 against *Aspergillus fumigatus* and *Candida albicans*, Jundishapur J. Microbiol. 8 (9) (2015) e26381.
[40] G.R. Teodoro, K. Ellepola, C.J. Seneviratne, C.Y. Koga-Ito, Potential use of phenolic acids as anti-*Candida* agents: a review, Front. Microbiol. 6 (2015) 1420.
[41] B. Alberts, A. Johnson, J. Lewis, D. Morgan, M. Raff, K. Roberts, et al., Artmed (Ed.), Molecular Biology of the Cell, 6th edition, vol. 18, 2017, pp. 1021–1034 Porto Alegre.
[42] P.V. AshaRani, G.L.K. Mun, M.P. Hande, S. Valiyaveettil, Cytotoxicity and genotoxicity of silver nanoparticles in human cells, ACS Nano 3 (2009) 279–290.
[43] V.M. Longo, C.C. de Foggi, M.M. Ferrer, A.F. Gouveia, R.S. Andre, W. Avansi, et al., Potentiated eléctron transference in α-Ag_2WO_4 microcrystals with Ag nanofilaments as microbial agent, J. Phys. Chem. A 118 (2014) 5769–5778.
[44] S. Chernousova, M. Epple, Silver as antibacterial agent: ion, nanoparticles, and metal, Angew. Rev. 52 (2013) 1636–1653.